

# Measurement of small birefringence and loss in a nonlinear single-mode waveguide

Daniel J. Rogers,<sup>1,a)</sup> Christopher J. K. Richardson,<sup>2</sup> Julius Goldhar,<sup>3</sup> and Charles W. Clark<sup>1</sup>

<sup>1</sup>Joint Quantum Institute, National Institute of Standards and Technology, 100 Bureau Drive, Gaithersburg, Maryland 20899, USA

<sup>2</sup>Laboratory for Physical Sciences, 8050 Greenmead Drive, College Park, Maryland 20740, USA

<sup>3</sup>Department of Electrical and Computer Engineering, University of Maryland, College Park, Maryland 20742, USA

(Received 27 January 2009; accepted 5 April 2009; published online 11 May 2009)

We design and fabricate a birefringent semiconductor waveguide for application to nonlinear photonics, demonstrating that it is possible to engineer a small birefringence into such a device using multiple core layers. We also demonstrate a simple technique to accurately determine small waveguide birefringence using a differential measurement, present useful methods for coupling light into and out of the device, and make estimates of coupling and linear device losses. © 2009 American Institute of Physics. [DOI: 10.1063/1.3124798]

## I. INTRODUCTION

Nonlinear optical processes in photonic waveguides are finding a myriad of new uses, from wavelength conversion<sup>1,2</sup> for all-optical routing to sources of entanglement for quantum communications.<sup>3</sup> Employing third-order nonlinear processes such as four-wave mixing has some distinct advantages over second-order processes for these applications; because the wavelength shifts are potentially smaller for  $\chi^{(3)}$  processes when compared to  $\chi^{(2)}$  processes, designing waveguides for such operation can be much more straightforward. However, one potential drawback to using  $\chi^{(3)}$  processes such as four-wave mixing is potential interference from noise due to Raman scattering.<sup>4</sup> Lin *et al.*<sup>5</sup> propose using birefringent phase matching to effectively separate Raman noise from four wave mixing-generated signals via polarization; the Raman scattered light is polarized orthogonally to the correlated photons of interest. However, for small detunings, this requires that the device exhibit a correspondingly small birefringence.

Birefringent phase matching is by no means a new technique. It has been used extensively for phase matching nonlinear processes in optical fibers.<sup>6</sup> However, fibers exhibit significant nonuniformity in birefringence introduced during fabrication,<sup>7</sup> limiting their nonlinear performance when using this technique. Because the semiconductor material described here is grown epitaxially, the birefringence induced by the layer structure in these devices is much more uniform, indicating that they should exhibit better nonlinear performance than comparable optical fibers.

In this article, we demonstrate the design, fabrication, and measurement of a waveguide with a small birefringence for application to nonlinear photonics. The device is an AlGaAs rib waveguide with a buried, multilayer core that creates a form birefringence<sup>8</sup> on the same order of magnitude as

observed strain effects in similar materials.<sup>9</sup> The measurement apparatus, based on the idea of a birefringent, or Lyot, filter<sup>10</sup> can measure birefringence to an index difference on the order of  $10^{-5}$ . The resulting device has potential application as a source of entangled photon pairs for quantum communication, but it can serve as a starting point for any nonlinear photonic device that uses birefringent phase matching.

## II. DEVICE DESIGN AND FABRICATION

### A. Design and model results

The intended application of the device was as a nonlinear source of correlated photons for quantum communications. The birefringent phase matching condition of the exploited nonlinearity dictated that we design a rib waveguide, pumped at 780 nm, with a core made of Al<sub>0.3</sub>Ga<sub>0.7</sub>As and a target birefringence of  $\delta n = n_x - n_y$  between  $10^{-4}$  and  $10^{-3}$ . We achieved the desired index difference via form birefringence induced in a core comprised of multiple layers with slightly different aluminum content. The resulting difference in the material's refractive index, along with the relative thickness of each layer, determined the birefringence of the overall core region. Assuming the form birefringence is small, we can use the formalism of Ref. 8 to predict the contribution of the form birefringence in the core  $\delta n_{\text{form}}$  to the overall birefringence of the device

$$\delta n_{\text{form}} \approx \frac{1}{2n_1(\lambda)} \cdot \frac{f_1 f_2 (n_1(\lambda)^2 - n_2(\lambda)^2)^2}{(1 + f_1)n_2(\lambda)^2 + f_2 n_1(\lambda)^2}, \quad (1)$$

where  $f_1 = 50/(50+70)$  and  $f_2 = 70/(50+70)$  are the fractional thicknesses of one full period of the alternating core layers, as defined in Fig. 1, and  $n_1(\lambda)$  and  $n_2(\lambda)$  are their respective indices of refraction.

The final design is shown in Fig. 1. Inset is the solution to the lowest-order TE mode as computed by a full-vector finite-difference modesolver.<sup>11</sup> The predictions for the birefringence are shown in Fig. 2. The form birefringence was

<sup>a)</sup>Electronic mail: daniel.rogers@nist.gov.

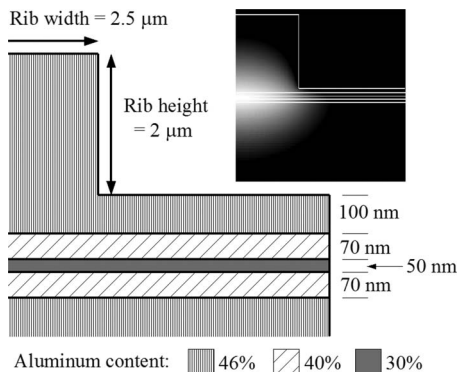


FIG. 1. Schematic, not to scale, of the right half of a symmetric cross-section of the birefringent waveguide, showing the dimensions and aluminum concentrations of the cladding and multiple core layers. The computational solution for the lowest-order TE mode, inset, is also symmetric about the left edge of the image.

calculated from Eq. (1) along with the Sellmeier coefficients in Ref. 9. The total birefringence was computed by multiple simulations with the mode solver at different wavelengths, also incorporating the Sellmeier equations in Ref. 9 governing the index of each layer. The contribution of the waveguide birefringence, due to the anisotropy of the mode shape, was inferred as the difference between the total birefringence from the mode solver and the form birefringence of the core calculated from Eq. (1). Note that the dimensions and indices used in the simulation were corrected for the measured results of the actual device fabrication.

## B. Device fabrication and characterization

The material for the device was epitaxially grown on a GaAs substrate<sup>12,13</sup> and verified using x-ray diffraction. The aluminum percentages of the AlGaAs layers were grown to within 3% of the target, and the relative aluminum content between layers was grown to better than 1% of the target. The defect rate of the final growth was less than  $100 \text{ cm}^{-2}$ .

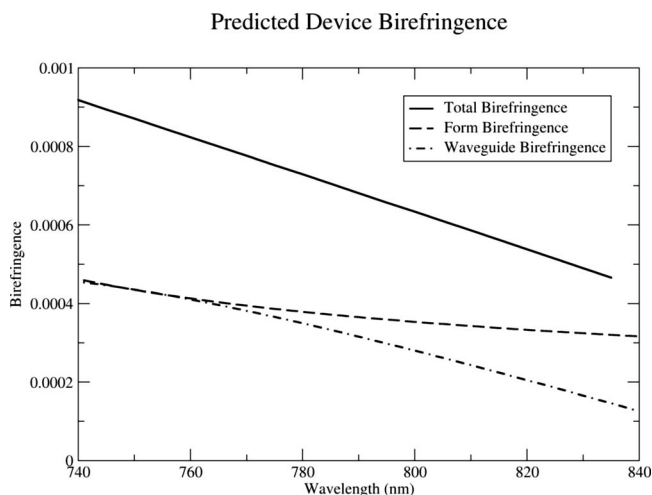


FIG. 2. Contributions of different effects leading to the total device birefringence, as determined from mode solving software (Ref. 11). The form birefringence was calculated using the formalism in Ref. 8 and the Sellmeier coefficients from Ref. 9.

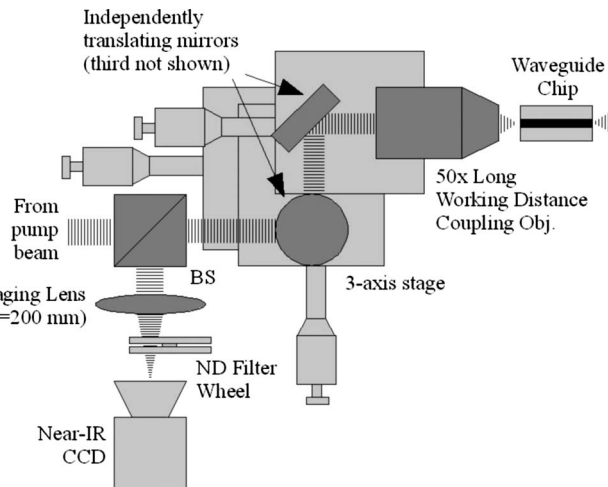


FIG. 3. Schematic of the input coupling stage with integrated microscope. A similar stage, not shown, is used on the output side of the device and is aligned to the detector.

The final rib structure was fabricated using an inductive coupled plasma etch;<sup>14</sup> the rib width was measured via scanning electron microscopy to be  $2.62 \mu\text{m}$ .

## C. Light coupling

One of the most challenging aspects of working with single-mode photonic waveguides is the task of coupling light into and out of the device. Even in devices such as ring resonators, coupling is often the single most limiting factor in performance.<sup>15</sup> The birefringence measurement outlined in this article used simple microscope objectives that were matched in numerical aperture to the waveguide, while the coupling was monitored using an overhead video microscope. Though this method is rather minimal, it was effective enough for the purposes of that measurement. However, for measurements requiring more precise positioning, including nonlinear measurements with high-power beams that risk damaging the device or quantum optical measurements involving very low light levels, it is important to use a more sophisticated coupling technique. Figure 3 depicts a more advanced free-space coupling setup that incorporates a confocal video microscope on both the input and output beam paths.<sup>16</sup> On the input side, this arrangement enables positioning of the high-power pump beam to within 30 nm in order to avoid damage to the substrate or other absorbing features on the chip. On the output side, an equivalent system is aligned to a detector using a HeNe laser. The presence of this second microscope in the output coupling path allows for the detection of signals on the single-photon level that are too small to observe visually but are still within the sensitivity of single-photon detectors; by visually aligning the confocal microscope to the output facet of the device, one can ensure that the small signals are aligned to the detector as well. Because these confocal arrangements give a real-time image of both the input facet and output facet, it is also possible to qualitatively monitor the coupling alignment in real time. Furthermore, the free-space nature of the optical path allows for the easy modification of optics within the setup, allowing one to perform a variety of measurements with a single sys-

tem. While this setup was not required for the birefringence measurements described here, it was vital for the loss measurements and subsequent nonlinear measurements performed later.

### III. BIREFRINGENCE MEASUREMENT

To predict where the nonlinear process of interest was phase matched, we first measured the actual birefringence of the device. A number of methods exist to determine the birefringence of a waveguide, but few meet the accuracy required for the small birefringence of the device considered. The simplest method involves an imaging technique that examines scattered light out-of-plane similar to that described in Ref. 17.  $45^\circ$  polarized light at the input will split into two components along the polarization axes; since the medium is birefringent, the resulting polarization will rotate along the length of the device. Because light scatters differently from impurities depending on its polarization, the rotation should result in variations in out-of-plane scattered light along the length of the device. Given the device parameters, we would expect to see approximately 1.5 full periods of scattered intensity variation in 9 mm. However, after careful observation, it is apparent that loss, speckle, the nonlinear response of the charge coupled device, and low intensity make this technique impractical. The expected rotation period is on the order of 5 mm; the device loss, estimated to be 5 dB/cm, resulted in a significantly reduced fringe visibility along the length of the device, making accurate birefringence measurements involving the observation of more than one fringe increasingly difficult. Furthermore, since the technique relies on the uniform presence of impurities in the semiconductor, fabricating better devices also makes the measurement more difficult.

Another approach involves a more direct measurement of the ordinary and extraordinary indices of refraction. Since the waveguide facets are uncoated, they offer 30% reflection of the input field at each interface. One possible measurement technique involves comparing the Fabry–Pérot fringe spacing for light polarized along the two polarization axes, directly giving us the difference in index of refraction.<sup>18</sup> However, for a 9 mm long device with the predicted birefringence, the expected fringe spacing is on the order of 0.1  $\mu\text{m}$  at  $\lambda=780$  nm. This corresponds to a difference in free spectral range (FSR) of 50 MHz. While this can, in principle, be measured using a heterodyne technique, the full width at half maximum of such a resonance with 30% facet reflections is approximately 4 GHz. This is much broader than the difference in FSR, making a measurement of this type impractical.

Thus we chose to employ a third technique, also based on a birefringent filter, but exploiting variations in wavelength rather than propagation distance. A number of similar techniques have been demonstrated.<sup>19–22</sup> However, none of these techniques involve a broadband light source, and many are limited in accuracy to a birefringence greater than that predicted for this device.

In our apparatus, the birefringent medium under test is placed between two crossed polarizers oriented at  $\pm 45^\circ$  to the polarization axes. The form birefringence of the medium

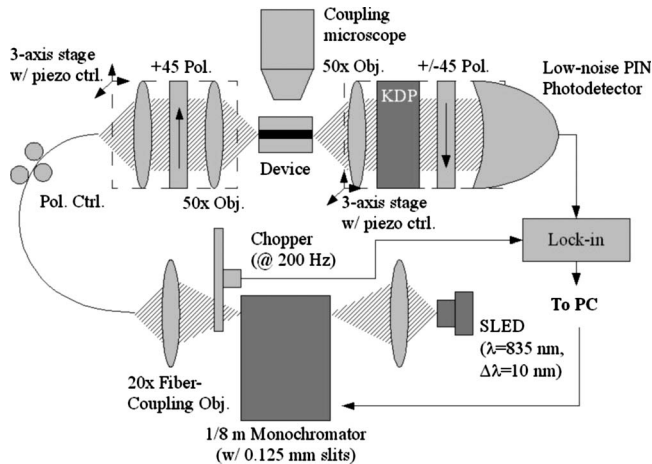


FIG. 4. Modified birefringent filter setup used to measure the waveguide birefringence.

rotates different wavelengths by different amounts. When broadband light is launched through the polarizer, spectral fringes result at the output of the analyzer with spacing dependent on the material birefringence.<sup>10</sup> Because the birefringence of the device is so small, the fringe spacing for this simple setup is on the order of 100 nm, larger than the spectral width of most bright, broadband sources. However, by employing a second crystal with a larger birefringence, we are able to make a differential measurement when the device under test is introduced into the system. This technique allows for more accurate determination of small birefringence.

#### A. Apparatus and procedure

The setup, shown in Fig. 4, consists of broadband light from a superluminescent light-emitting diode, centered at 835 nm with a width of approximately 10 nm. It is filtered through a computer-controlled, 1/8 m monochromator with 0.125 mm slits, mechanically chopped at 200 Hz, and launched through a  $+45^\circ$  thin-film polarizer into the waveguide using a  $50\times$  microscope objective. The waveguide output is coupled through a 4.8 mm long potassium dihydrogen phosphate (KDP) crystal via another objective lens and collimated. The polarization axes of the KDP are oriented to match those of the waveguide. The output is then passed through a thin-film analyzer oriented at  $-45^\circ$  and detected using a low-noise *PIN* photodiode. The diode output is detected via a lock-in amplifier synchronized to the optical chopper and recorded on a PC. The measurement procedure consists of making a spectral scan first with the waveguide in place, then rotating the analyzer by  $90^\circ$ , resulting in fringes that are inverted. This step enables accurate determination of the fringe spacing. Finally, the waveguide is removed, the two objectives are coupled together, and a second pair of scans, again rotating the analyzer, is made with only the KDP in place. The results are shown in Fig. 5.

#### B. Results and error analysis

We can predict the relationship between the fringe spacing and the birefringence by simply considering the product

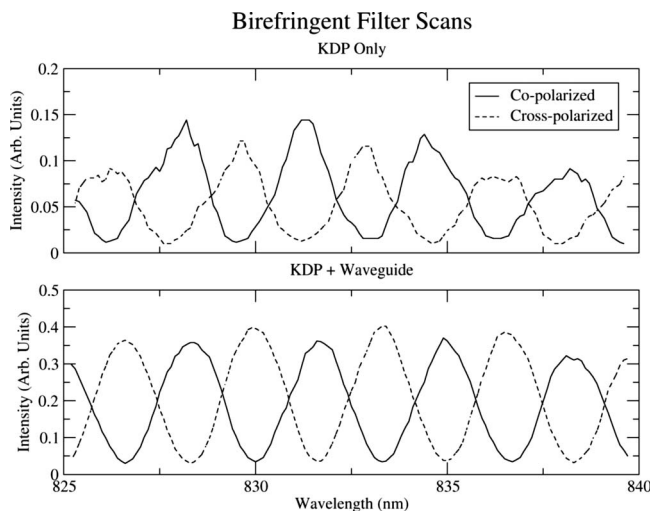


FIG. 5. Birefringent filter scans with and without the waveguide in place.

of the Jones matrices of the various components along the optical path. The Jones matrix for a typical birefringent element is given by

$$\mathbf{J} = \begin{pmatrix} e^{i\pi\delta nL/\lambda} & 0 \\ 0 & e^{-i\pi\delta nL/\lambda} \end{pmatrix}, \quad (2)$$

where  $\delta n$  is the birefringence of the element and  $L$  is the propagation length. For the apparatus described above, we can compute the product of the Jones matrices of the various elements to obtain

$$\begin{aligned} I(\lambda) &= |\vec{A}_{-45^\circ}^T \cdot \mathbf{S}^{-1} \mathbf{J}_{\text{KDP}} \mathbf{S} \cdot \mathbf{R}^{-1} \mathbf{J}_{\text{WG}} \mathbf{R} \cdot \vec{P}_{+45^\circ}|^2 \\ &= 2 \sin^2 \left[ \frac{k}{2} (\delta n_0 L_0 + \delta n L) \right], \end{aligned} \quad (3)$$

where  $\mathbf{J}_{\text{WG}}$  and  $\mathbf{J}_{\text{KDP}}$  are the Jones matrices for the waveguide and KDP, respectively.  $\delta n_0$  and  $\delta n$  are the birefringence of the KDP and the waveguide, respectively, and  $L_0$  and  $L$  are their respective lengths. The rotation matrices  $\mathbf{R}$  and  $\mathbf{S}$  are assumed to be trivial in this computation since all of the birefringent elements are aligned.  $\vec{P}_{+45^\circ}$  is the Jones vector for light launched at  $+45^\circ$  and  $\vec{A}_{-45^\circ} = 1/\sqrt{2} \begin{pmatrix} 1 \\ -1 \end{pmatrix}$  represents the analyzer oriented at  $-45^\circ$ . For a perfect device, we assume  $\vec{P}_{+45^\circ} = 1/\sqrt{2} \begin{pmatrix} 1 \\ 1 \end{pmatrix}$ . However, since our device has a noncircular mode, there must be non-negligible polarization-dependent loss (PDL). PDL enters into the analysis by substituting a new Jones vector  $\vec{P}'_{+45^\circ} = 1/\sqrt{2} \begin{pmatrix} \eta_x \\ \eta_y \end{pmatrix}$  for  $\vec{P}_{+45^\circ}$ , where  $\eta_x$  and  $\eta_y < 1$  are the coupling efficiencies of the  $x$ - and  $y$ -polarized modes. The resulting intensity is given by

$$I'(\lambda) = \frac{1}{4} \{ \eta_x^2 + \eta_y^2 - 2\eta_x\eta_y \cos[k(\delta n_0 L_0 + \delta n L)] \}. \quad (4)$$

We see from Eq. (4) that incorporating  $\vec{P}'_{+45^\circ}$  reduces the fringe visibility but does not change their spacing. Furthermore, any wavelength dependence will result in an envelope to the fringes but still will not affect the fringe spacing.

Additionally, small errors in alignment, equivalent to small changes in  $\mathbf{R}$  and  $\mathbf{S}$  from the trivial  $0^\circ$  case, will have a minimal impact on fringe spacing. While a detailed analytical expression for the size of these errors is a rather complicated function of the misalignment angles, we can ap-

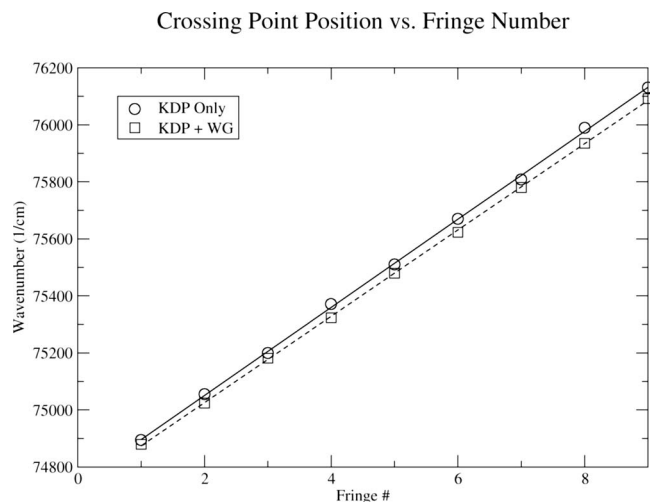


FIG. 6. Slopes showing difference in fringe spacing due to waveguide birefringence. Error bars in the points are too small to plot.

proximate the order of the effect by considering only a misalignment between the polarization axes of the two birefringent media. The eigenvalues of the product  $\mathbf{S}^{-1} \mathbf{J}_{\text{KDP}} \mathbf{S} \times \mathbf{J}_{\text{WG}}$  for a small misalignment  $\theta$  contain terms periodic in  $k/2(\delta n_0 L_0 + \delta n L)$  as well as additional terms proportional to  $\theta^2$ . The nulls in the observed fringes correspond to points where these eigenvalues are equal, so the fringe spacing will have the same period as the eigenvalues. Since the change in the eigenvalue period varies as  $\theta^2$ , we can assume that errors in the fringe spacing are on the same order in the misalignment angle. To illustrate the nature of the effect, Fig. 7 shows a calculated fringe incorporating misalignment in both the KDP and waveguide of up to  $10^\circ$ . As the plot illustrates, errors smaller than  $10^\circ$  have negligible effect on the fringe spacing compared to the shift introduced by the waveguide's birefringence, indicating that the measurement is rather robust in the presence of small misalignments in the polarization axes.

Note that the fringe spacing derived in Eq. (3), excluding effects of PDL and misalignment, is linear in wavenumber and proportional to the total birefringence between the polarizer and analyzer. To determine the fringe spacing, we plot the wavenumbers of the crossing points between the normal and inverted fringes versus the fringe number, as shown in Fig. 6. The slope of the resulting lines,  $\Delta K$  and  $\Delta K_0$ , correspond to the fringe spacings with and without the waveguide in place. From these, we can first compute the measured birefringence of the KDP alone using the following expression:

$$\delta n_0 = \frac{\pi}{L_0 \Delta K_0}. \quad (5)$$

$\Delta K_0$  was determined to be  $154.3 \pm 1.2 \text{ cm}^{-1}$ , indicating a birefringence of  $\delta n_0 = 0.042 \pm 0.001$ . This measurement matches published results for KDP to better than 5%.<sup>23</sup> Next, we can determine the birefringence of the waveguide alone using the expression

## Computed Effect of Misalignment on Fringe Spacing and Visibility

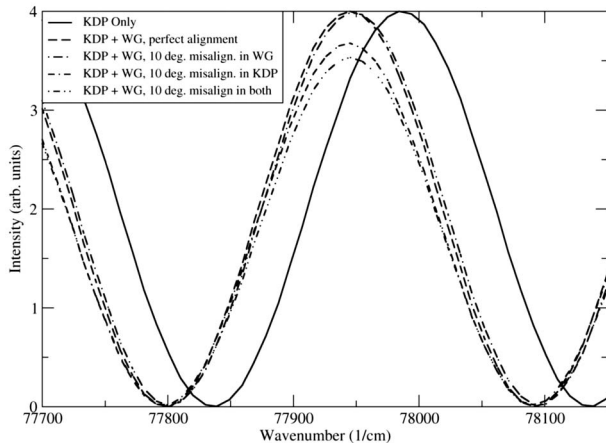


FIG. 7. Calculated fringes showing the effects of misalignment of the polarization axes of the device (WG) and the KDP crystal on the measurement. Shown in the plot are predicted fringes for a measurement of the KDP alone of the perfectly aligned waveguide and KDP together, and of both components together with various combinations of  $10^\circ$  misalignments. While fringe visibility can be significantly affected by the misalignment, the fringe spacing remains unperturbed to within 5% of the spacing.

$$\delta n = \left| \frac{\pi}{L\Delta K} - \frac{L_0}{L} \delta n_0 \right|. \quad (6)$$

The absolute value accounts for the possibility that the slow and fast axes are inverted between the waveguide and the KDP crystal, possibly resulting in a subtractive, rather than additive, birefringence. This is equivalent to the matrices  $\mathbf{R}$  and  $\mathbf{S}$  representing a  $90^\circ$  rotation rather than the trivial  $0^\circ$  case, resulting in a reversal of the terms in Eq. (6).

The slope  $\Delta K$  was determined to be  $151.4 \pm 0.7 \text{ cm}^{-1}$ , approximately six standard deviations smaller than  $\Delta K_0$ . The resulting birefringence of the waveguide is  $\delta n = 0.00044 \pm 0.00005$ , which closely matches the value of 0.00046 predicted by the modeling at 835 nm. Furthermore, even though this value is on the same order as birefringence due to strain introduced during material growth,<sup>9</sup> the model does not include strain effects. We can infer that strain is likely not a significant factor, as strained layers in the material constitute a small volume fraction and should have minimal impact. Thus the birefringence is primarily determined by the multilayer core structure.

#### IV. LOSS MEASUREMENTS

Power measurements were made using the free-space coupling setup shown in Fig. 3. Because the free-space coupling scheme allowed access to the optical path, power measurements were made both before the input coupling objective and after the output coupling objective with a large-area power meter calibrated for linearity. Neglecting any small loss within the objectives themselves, the ratio between the two powers provided a good measure of the insertion loss. With this setup, we achieved  $13 \pm 1$  dB insertion loss. We further measured the linear loss of the device by estimating the decay in scattered light from plan-view microscope im-

ages. Fitting an exponential to the image resulted in an estimated 5 dB of linear loss in the 9 mm device, indicating a coupling loss of 8 dB.

#### V. CONCLUSIONS

In this article, we have demonstrated the ability to design and fabricate a waveguide to a specific, small birefringence. We have also demonstrated a novel modification to a traditional method of measuring birefringence. This modification enables the accurate determination of small birefringence in photonic devices. If birefringent phase matching becomes the preferred method of exploiting third-order optical nonlinearities without interference from Raman noise, then this technique will become useful in predicting the phase-matched wavelengths. These measurements constitute a starting point for the design of a birefringent, nonlinear waveguide for correlated photon generation or wavelength conversion.

#### ACKNOWLEDGMENTS

We gratefully acknowledge the support of the fabrication staff at the Laboratory for Physical Sciences for their generous assistance in fabricating the devices used in this effort, as well as Professor Tom Murphy for providing the mode solving code and for keen experimental advice. We would also like to thank Dr. Michael Anderson of Vescent Photonics for suggestions regarding birefringence measurement techniques, Dr. Richard Mirin of NIST Boulder for assistance with the stage design, Dr. Christophe Couteau of the University of Waterloo for helpful suggestions regarding coupling, and Dr. Joshua Bienfang, Dr. Alessandro Restelli, and Dr. Alan Migdall of NIST Gaithersburg for generally fruitful discussions.

- <sup>1</sup>M. A. Foster, A. C. Turner, R. Salem, M. Lipson, and A. L. Gaeta, *Opt. Express* **15**, 12949 (2007).
- <sup>2</sup>R. Espinola, J. Dadap, J. Richard Osgood, S. McNab, and Y. Vlasov, *Opt. Express* **13**, 4341 (2005).
- <sup>3</sup>J. E. Sharping, K. F. Lee, M. A. Foster, A. C. Turner, B. S. Schmidt, M. Lipson, A. L. Gaeta, and P. Kumar, *Opt. Express* **14**, 12388 (2006).
- <sup>4</sup>X. Li, J. Chen, P. Voss, J. Sharping, and P. Kumar, *Opt. Express* **12**, 3737 (2004).
- <sup>5</sup>Q. Lin, F. Yaman, and G. P. Agrawal, *Opt. Lett.* **31**, 1286 (2006).
- <sup>6</sup>R. H. Stolen, M. A. Bosch, and C. Lin, *Opt. Lett.* **6**, 213 (1981).
- <sup>7</sup>J. Pezeshki, H. Mandelburg, M. Saylor, and J. Goldhar, Proceedings of the Conference on Lasers and Electro-Optics, 2003 (unpublished), pp. 1011–1013.
- <sup>8</sup>M. Born and E. Wolf, *Principles of Optics* (Cambridge University, New York, 1999).
- <sup>9</sup>S. Gehrsitz, F. K. Reinhart, C. Gourgon, N. Herres, A. Vonlanthen, and H. Sigg, *J. Appl. Phys.* **87**, 7825 (2000).
- <sup>10</sup>W. Stolz, Ph.D. thesis, University of Stuttgart, 1986.
- <sup>11</sup>A. Fallahkhair, K. Li, and T. Murphy, *J. Lightwave Technol.* **26**, 1423 (2008).
- <sup>12</sup>J. J. R. Arthur, *J. Appl. Phys.* **39**, 4032 (1968).
- <sup>13</sup>R. Fischer, J. Klem, T. J. Drummond, R. E. Thorne, W. Kopp, H. Morkoç, and A. Y. Cho, *J. Appl. Phys.* **54**, 2508 (1983).
- <sup>14</sup>J. W. Lee, M. W. Devre, B. H. Reelfs, D. Johnson, J. N. Sasserath, F. Clayton, D. Hays, and S. J. Pearton, *J. Vac. Sci. Technol. A* **18**, 1220 (2000).

- <sup>15</sup>R. Grover, P. P. Absil, V. Van, J. V. Hryniewicz, B. E. Little, O. King, L. C. Calhoun, F. G. Johnson, and P.-T. Ho, *Opt. Lett.* **26**, 506 (2001).
- <sup>16</sup>R. H. Hadfield, M. J. Stevens, S. S. Gruber, A. J. Miller, R. E. Schwall, R. P. Mirin, and S. W. Nam, *Opt. Express* **13**, 10846 (2005).
- <sup>17</sup>A. L. Bajor, *Rev. Sci. Instrum.* **66**, 2977 (1995).
- <sup>18</sup>N. Ponnampalam, R. DeCorby, H. Nguyen, P. Dwivedi, C. Haugen, J. McMullin, and S. Kasap, *Opt. Express* **12**, 6270 (2004).
- <sup>19</sup>S. Jacobsson and S. Hard, *Rev. Sci. Instrum.* **53**, 1012 (1982).
- <sup>20</sup>M. Yamada, *Rev. Sci. Instrum.* **64**, 1815 (1993).
- <sup>21</sup>B. Wang and T. C. Oakberg, *Rev. Sci. Instrum.* **70**, 3847 (1999).
- <sup>22</sup>Y. Nishida and M. Yamanaka, *Rev. Sci. Instrum.* **72**, 2387 (2001).
- <sup>23</sup>F. Zernike, Jr., *J. Opt. Soc. Am.* **54**, 1215 (1964).